CHEMISTRY
A EUROPEAN JOURNAL

DOI: 10.1002/chem.200600748

Protonated Heme

Barbara Chiavarino,[a] Maria Elisa Crestoni,[a] Simonetta Fornarini,*[a] and Carme Rovira*[b]

Abstract: The ions formally corresponding to protonated heme [Fe^{II}–hemeH]$^+$ have been obtained by collision-induced dissociation from the electrospray ionization of microperoxidase (MP11) and their gas-phase chemistry has been studied by FTICR mass spectrometry. H/D-exchange reactions, used as a tool to gain information on the protonation sites in polyfunctional molecules, show that labile hydrogens pertain to the propionyl substituents at the periphery of the protoporphyrin IX. Several conceivable isomers for protonated heme have been evaluated by density functional theory. The most stable among the species investigated is the one corresponding to protonation at the β carbon atom of a vinyl group, yielding a proton affinity (PA) value for [Fe^{II}–heme] of 1220 kJ mol^{-1}. This high PA is consistent with the inertness of the hydrogen atoms at the protonation site towards H/D exchange with ND_3 and CD_3CO_2D. Peculiar features of this [Fe^{II}–hemeH]$^+$ isomer emerge by analysis of its electronic structure, showing that the vinyl group undergoing formal protonation has gained significant radical character due to electron transfer from the metal center. As a consequence, the iron atom acquires partial iron(III) character and none of the two formal descriptions [Fe^{II}–hemeH$^+$] and [Fe^{III}–hemeH$^{\bullet}$]$^+$ alone may adequately illustrate the protonated heme ion. In agreement with this description, the reactivity of protonated heme presents dual facets, resembling iron(III) in some aspects and iron(II) in others. On the one hand, protonated heme behaves like [Fe^{III}–heme]$^+$ ions in H/D-exchange reactions. On the other, it shows markedly decreased reactivity towards the addition of ligands with the notable exception of NO, in line with the high affinity shown by iron(II) complexes towards this molecule, NO, of key biological role.

Keywords: density functional calculations · FTICR mass spectrometry · ion-molecule reactions · iron · molecular dynamics

Introduction

The prosthetic group constituted of an iron(II/III)–protoporphyrin IX complex is the core of heme proteins, a vast family of metalloproteins promoting such diverse functions as dioxygen transport and storage, electron transfer, oxidation of organic compounds, and hydrogen peroxide disproportion.[1,2] The versatile functions presented by heme groups in biological and synthetic systems has also made these units an interesting choice for incorporation in monolayers on solid supports, for the development of sensing devices towards simple inorganic molecules, and for the design of building blocks to construct solids with specific properties.[3] In heme proteins, it is well established that the protein matrix controls the reactivity of the prosthetic group both affecting the coordination environment and directing long-range interactions.[4] For this reason the protein composition and structural organization are important factors in regulating the heme–protein activity. Sustained efforts are aimed at dissecting the relative weight of the various factors contributing to the properties of the heme protein, some of which utilize artificial model systems.[5–8] It is conceivable, however, that the intrinsic features of the heme group may be best ascertained in the gas phase, in the lack of both a protein matrix and a solvation medium. When considered in an isolated state, theoretical approaches to the structure and func-

[a] Dr. B. Chiavarino, Prof. M. E. Crestoni, Prof. S. Fornarini
Dipartimento Studi di Chimica e Tecnologia delle Sostanze Biologicamente Attive, Università di Roma "La Sapienza"
P.le A. Moro 5, 00185 Roma (Italy)
Fax: (+39) 06-4991-3602
E-mail: simonetta.fornarini@uniroma1.it

[b] Dr. C. Rovira
Centre de Recerca en Química Teòrica
Parc Científic de Barcelona, Josep Samitier 1–5
08028 Barcelona (Spain)
Fax: (+34) 93-403-7225
E-mail: crovira@pcb.ub.es

Supporting information for this article is available on the WWW under http://www.chemeurj.org/ or from the author.

tion of heme-type groups may be applied in a straightforward way,[7,9] without any need to account for a protein/solvent environment.[10] The structural features and the electronic properties of the heme group or of heme models have been the topic of innumerable studies based on various computational approaches.[11] Significant contributions to the understanding of heme-group chemistry have been a result of theoretical investigations of the iron–porphyrin complexes with diatomic molecules, such as O_2, CO, and NO by using density-functional-based calculations.[11a,12] The FeP complex (in which P is the dianion of porphine) has been frequently used as a simplified model of the heme group, relying on the fact that porphyrin substituents have been shown not to significantly affect the electronic structure of iron–porphyrin complexes,[13] whereas the axial ligands are confirmed to play a role in the biological activity of the heme unit.[14] Similar theoretical approaches have also been used to study the process of ligand binding and the effect of porphine substituents on the ligand binding properties.[15]

The iron(II)–protoporphyrin IX complex [Fe^{II}–heme] is itself neutral and gas-phase studies using MS techniques normally handle charged species. A few charged iron–porphyrin complexes have been produced by various means.[16] Iron porphyrin ions may be synthesized in the gas phase by the metallation reaction of porphyrins with Fe^+ ions obtained by laser ablation.[17] The metallation of the porphyrin ring system has been extensively studied both in solution and in biological systems and its mechanism has been recently examined theoretically.[18] Alternatively, electrospray ionization (ESI) affords a convenient source of iron–porphyrin ions, which have been investigated for their binding properties to ligands coordinating to the vacant axial sites.[19] The selected ligands include nitric oxide,[19a] nitrogen bases,[19b] and various neutrals possessing functionalities that are present in a protein backbone.[19c] Both kinetic and thermodynamic parameters for the iron–porphyrin ion association reaction in the gas phase have been reported. ESIMS has also been used to gain information on the complexes formed in solution between iron–porphyrin ions and ligands, including antimalarial drugs.[20] However, an important issue affecting the properties of iron–porphyrin species, namely the oxidation state of iron, has not been specifically addressed. For example, only [Fe^{III}–heme]$^+$ ions have been examined to establish a relative (and absolute) scale of free energies of association to a series of model compounds.[19c] One problem regarding gaseous [Fe^{II}–heme] is the lack of net charge. A positive charge may be imparted on Fe^{II}–porphyrin complexes by protonation of basic substituents on the tetrapyrrole ring, as obtained by ESI of iron tetrapyridylporphyrin chloride.[19a] The present study is aimed at characterizing the [Fe^{II}–hemeH]$^+$ ion, formally corresponding to protonated [Fe^{II}–heme], in which the naked prosthetic group is perturbed only by the presence of an additional proton. [Fe^{II}–hemeH]$^+$ has been obtained by ESI of appropriate precursors and its ion chemistry has been investigated by FTICR mass spectrometry. The association reactions with exemplary neutrals and H/D-exchange reactivity have been investigated, thus allowing a comparative assay of [Fe^{II}–hemeH]$^+$ and [Fe^{III}–heme]$^+$ ions. At the same time, a theoretical study by using density functional theory (DFT) has provided an insight into the equilibrium geometries and electronic structure of formal [Fe^{II}–hemeH]$^+$ ions.

Results

Gas-phase ion chemistry: [Fe^{III}–heme]$^+$ ions are obtained directly by submitting to ESI a hemin chloride [Fe^{III}–heme$^+$ Cl^-] solution so that the whole process implies the transfer of ions from solution to the gas phase with concomitant desolvation.[19c] A different entry is, however, needed to produce gaseous [Fe^{II}–hemeH]$^+$ ions. These species are reported to be the collision-induced dissociation (CID) products of ionized cytochrome c, a heme protein containing a covalently bound Fe^{III}–heme group.[21] In a study of the dissociation reactions of cytochrome c ions, the formation of a fragment ion in the reduced state has been ascribed to an electrochemical reduction of the protein occurring in a nanoelectrospray capillary.[22] However, the infrared multiphoton dissociation, a particularly "soft" activation technique, of cytochrome c ions is also found to release [Fe^{II}–hemeH]$^+$ ions, showing that the iron center of the heme group formally gains one electron during dissociation.[23] If cytochrome c is a useful source of [Fe^{II}–hemeH]$^+$ ions, it is possible that a peptide fragment of the protein may display the same behavior. Indeed abundant [Fe^{II}–hemeH]$^+$ ions are obtained when microperoxidase (MP11, the heme undecapeptide derived from enzymatic cleavage of cytochrome c) is submitted to ESI. A high capillary to skimmer potential difference is applied to promote CID. In this way, the problem of obtaining [Fe^{II}–hemeH]$^+$ ions by protonation of [Fe^{II}–heme] is circumvented, a neutral that would not be easy to handle in our apparatus. In forming [Fe^{II}–hemeH]$^+$ ions by either route, the question rises as to where the site is on which the additional hydrogen is attached. This problem has been addressed both by experiment and by theoretical calculations.

H/D exchange: H/D-exchange reactions are a useful probe of ionic structures and provide a valuable tool for the study of both positively and negatively charged species.[24] The efficiencies for the isotope-exchange reaction are found to correlate with the energetics of formation of the association complex between the ion and the exchange reagent, at least within a wide range of relatively simple species.[25] Renewed interest in H/D-exchange reactions is due to their use as a tool to provide information on highly complex species, such as protonated peptides and proteins.[26,27] The reactivity of [Fe^{II}–hemeH]$^+$ ions towards H/D-exchange has been assayed and compared with the reactivity behavior of [Fe^{III}–heme]$^+$ ions. D_2O, CD_3CO_2D, and ND_3 have been used as H/D-exchange reagents, by introduction to the FTICR cell at constant pressure and enabling the ESI-formed ions to react for variable delay times as long as few hundred seconds. The results outlined in Table 1, show that D_2O is not

Table 1. H/D-exchange rates for heme cations with gaseous reagents.

Reactant ion	Exchange reagent	k_{exp}[a]	Φ[b]	Observed number of incorporated D atoms
$[Fe^{II}$–hemeH$]^+$	D_2O	–	–	0
$[Fe^{III}$–heme$]^+$	D_2O	–	–	0
$[Fe^{II}$–hemeH$]^+$	CD_3CO_2D	0.73 (1.2, 0.62) (*1.8*, *1.9*)	6.2	2
$[Fe^{III}$–heme$]^+$	CD_3CO_2D	1.42 (1.9, 1.1) (*2.9*, *3.3*)	12.0	2
$[Fe^{III}$–heme-$(OCH_3)]^+$	CD_3CO_2D	0.92	8.0	1
$[Fe^{II}$–hemeH$]^+$	ND_3	5.81 (11.5, 8.9) (*13.4*, *14.8*)	37.3	2
$[Fe^{III}$–heme$]^+$	ND_3	9.57 (10.1, 8.4) (*11.8*, *14.0*)	61.3	2
$[Fe^{II}$–hemeH$]^+$[c]	ND_3	n.a.	n.a.	2
$[Fe^{III}$–heme$]^+$[c]	ND_3	n.a.	n.a.	2

[a] Phenomenological rate constant for the incorporation of the first D atom, in units of 10^{-10} cm^3 molecule^{-1} s^{-1}, at the temperature of the FTICR cell of 300 K. Values for the rate constants of the two sequential exchange steps as obtained by the KinFit program are given in parentheses. When these values are corrected by statistical factors accounting for the number of H and D atoms involved in each elementary step (see text), the rate constant values are given in italics. [b] $\Phi = k_{exp}/k_{coll} \times 100$. k_{coll} is evaluated by using the parameterized trajectory theory.[30] [c] The reactant ion in these experiments is a d_2 ion, as obtained by ESI of a solution in deuterated solvents. n.a. stands for "not applicable" because H/D incorporation does not proceed beyond the incorporation of two deuterium atoms that are already present in the reactant ion.

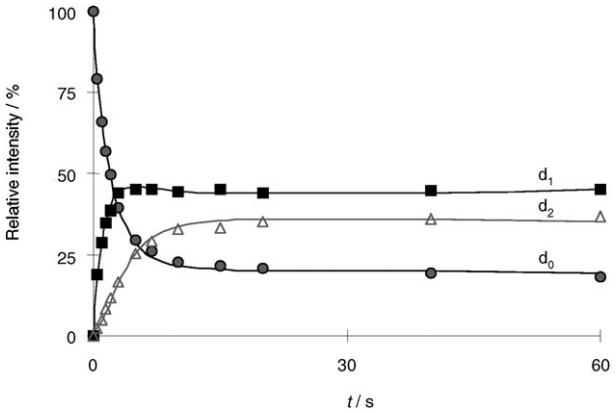

Figure 1. H/D-exchange kinetics for $[Fe^{II}$–hemeH$]^+$ ions reacting with CD_3CO_2D (1.7×10^{-7} mbar). The notation d_n refers to the number (n) of deuterium atoms incorporated into each species.

effective, at least in the present experimental setup. D_2O, with a proton affinity (PA) of 691 kJ mol^{-1},[28] is the least basic among the selected neutrals and this is a detrimental factor for activating D-atom incorporation within weakly acidic ions. In fact, for a large range of protonated simple compounds and exchange reagents the H/D-exchange rate is known to increase as the PA difference between the pair decreases, with a ΔPA limit of approximately 80 kJ mol^{-1}, inhibiting the exchange process.[25] In the case of protonated species that are increasingly complex, this limit is shifted to higher values, reaching approximately 250 kJ mol^{-1} for glycine oligomers, for example.[29] Adopting this same limit, the present result would suggest a PA value for $[Fe^{II}$–heme] greater than 941 kJ mol^{-1}. As shown by the data reported in Table 1, both CD_3CO_2D (PA = 783.7 kJ mol^{-1})[28] and ND_3 (PA = 853.6 kJ mol^{-1})[28] can activate the exchange of up to two hydrogen atoms. However, the ion abundance profiles (Figure 1) show that the D-incorporation reaction of $[Fe^{II}$–hemeH$]^+$ ions in the presence of CD_3CO_2D does not go to completion.

The relative ion abundances reach constant ratios resulting from the incomplete deuteration of the exchange reagent. In fact, in spite of a preliminary thorough equilibration of cell and inlets with D_2O, some residual source of exchangeable protons is probably responsible for the depleted D content (approximately 64%) in CD_3CO_2D with respect to the stated composition. The end ion abundances for the d_0, d_1, and d_2 species in Figure 1 (16, 45, and 39%, respectively) reflect the statistical distribution (13, 46, and 41%) expected for the exhaustive exchange of two labile hydrogen atoms. The incomplete deuteration of the reagent makes the H/D-exchange reaction reversible to a certain extent and therefore responding to Equation (1). The kinetics of the first exchange have been evaluated from the initial rates obtained from the semilogarithmic plots of the $[Fe^{II}$–hemeH$]^+$ ion (d_0) abundance versus time. The so-obtained rate constant, k_{exp}, and corresponding reaction efficiency (Φ) are given in Table 1. The time-dependence of the ion abundance of $[Fe^{II}$–hemeH$]^+$ (d_0) and the product ions incorporating one (d_1) or two (d_2) D atoms can also be analyzed by a kinetics fitting program[31] to yield the rate constants for the sequential H/D exchanges. The second-order rate constants k_1 and k_2 are given in parentheses in Table 1.

$$d_0 \overset{k_1}{\rightleftharpoons} d_1 \overset{k_2}{\rightleftharpoons} d_2 \qquad (1)$$

The exchange reactivity with CD_3CO_2D displayed by $[Fe^{III}$–heme$]^+$ is similar to the one shown by $[Fe^{II}$–hemeH$]^+$, both for the number of labile hydrogens and for the rate constant values, differing by less than a factor of two. The two ions behave similarly also with respect to ND_3 as the exchange reagent, both reacting distinctly faster, as expected based on the higher PA of ND_3. As shown by the time dependence of ion abundances for the $[Fe^{II}$–hemeH$]^+$ ions reaction with ND_3 displayed in Figure 2, the d_2 ion is by far the prevailing species, once a quasi-stationary state is reached.

As seen in the CD_3CO_2D reaction, the relative distribution of deuterated ions is in agreement with the D content of the exchange reagent, determined by internal ionization of the neutral inside the cell. In spite of the higher exchange rates, ND_3 also fails to deliver more than two D atoms. In a further effort to drive the ions towards a more extensive H/D exchange, both $[Fe^{III}$–heme$]^+$ and $[Fe^{II}$–hemeH$]^+$ have been produced by ESI using deuterated methanol as the sol-

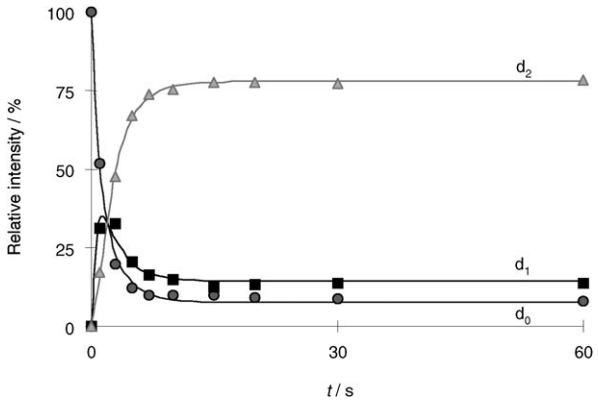

Figure 2. H/D-exchange kinetics for $[Fe^{II}–hemeH]^+$ ions reacting with ND_3 (3.0×10^{-8} mbar).

vent. Under these conditions, both ions are formed as d_2 species. However, they both fail to show any further D incorporation when they are exposed to ND_3 in the FTICR cell for several hundred seconds.

To gain information on the exchange site, the monomethyl ester derivative of $[Fe^{III}–heme]^+$ ($[Fe^{III}–heme(OCH_3)^+]$) has been tested and found to undergo just one H/D exchange when reacted with CD_3CO_2D (Table 1).

Ligand association reactions: The reaction of $[Fe^{III}–heme]^+$ with ND_3 and CD_3CO_2D leads not only to H/D-exchange products, but also to adduct ions. Ligand-addition reactions to $[Fe^{III}–heme]^+$ have been described[19] and the kinetic and thermodynamic features for the association of NH_3 have been reported for a series of model ligands.[19c] The ligand addition reactions to $[Fe^{III}–heme]^+$ studied in FTICR were found to obey second-order kinetics, first order in the reagent ion and first order in the neutral ligand. This finding was interpreted as evidence for a prevailing radiative mechanism for the stabilization of the adduct ion, primarily formed with excess internal energy due to the exothermicity of the association process.[19c] The free-energy change for NH_3 binding to $[Fe^{III}–heme]^+$ is equal to 69 kJ mol^{-1} and also carbonyl compounds, such as acetone and methyl acetate behave as effective ligands. Thus, it is not unexpected that acetic acid also displays ligand-binding behavior towards $[Fe^{III}–heme]^+$ [Eq. (2), $L=CD_3CO_2D$] with a second-order rate constant of 7×10^{-12} cm^3 molecule^{-1} s^{-1}, corresponding to a reaction efficiency of 0.6%. The rate of H/D exchange is approximately 20 times higher than that of the association reaction. The corresponding ratio is approximately 30 for the competing H/D exchange and association reactions of $[Fe^{III}–heme]^+$ with ND_3.

$$[Fe^{III}-heme]^+ + L \rightarrow [Fe^{III}-heme(L)]^+ \quad (2)$$

In contrast with the ligand-association reactivity of $[Fe^{III}–heme]^+$, $[Fe^{II}–hemeH]^+$ ions do not add to CD_3CO_2D nor to ND_3. Because the efficiency towards association to $[Fe^{III}–heme]^+$ correlates with the gas-phase basicity of the ligand,[19c] a strong base,[28] such as $(C_2H_5O)_3P$ has been reacted with $[Fe^{II}–hemeH]^+$ and found to undergo a fast association process [Eq. (3), $L=(C_2H_5O)_3P$], though not as fast as the reaction with $[Fe^{III}–heme]^+$.

$$[Fe^{II}-hemeH]^+ + L \rightarrow [Fe^{II}-hemeH(L)]^+ \quad (3)$$

Finally, given the central role that the heme group plays in NO binding and regulation, the reaction of NO with $[Fe^{II}–hemeH]^+$ is reported and evaluated against the remarkably high association efficiency displayed by $[Fe^{III}–heme]^+$. Table 2 summarizes the kinetic data for the association reactions.

Table 2. Ligand (L) association reactions of heme cations.

Reactant ion	L	k_{exp}[a]	Φ[b]
$[Fe^{III}–heme]^+$	CD_3CO_2D	0.07	0.6
$[Fe^{III}–heme]^+$	ND_3	0.34	2.0
$[Fe^{III}–heme]^+$	NO	0.22[c]	3.0[c]
$[Fe^{III}–heme]^+$	$(C_2H_5O)_3P$	13.0[c]	98[c]
$[Fe^{II}–hemeH]^+$	CD_3CO_2D	–	–
$[Fe^{II}–hemeH]^+$	ND_3	–	–
$[Fe^{II}–hemeH]^+$	NO	0.33	4.4
$[Fe^{II}–hemeH]^+$	$(C_2H_5O)_3P$	4.0	34

[a] Phenomenological rate constant for the ligand addition reaction, in units of 10^{-10} cm^3 molecule^{-1} s^{-1}, at the temperature of the FTICR cell of 300 K. [b] $\Phi=k_{exp}/k_{coll}\times100$. [c] See reference [19c].

The reactivity of $[Fe^{II}–hemeH]^+$ has been examined towards neutrals, such as dimethyldisulfide, that are known to behave as radical traps and have been used to characterize a free radical site in gaseous ions.[32] However, $[Fe^{II}–hemeH]^+$ failed to show any reactivity either with dimethyldisulfide or with potential donors of a hydrogen atom, such as tetrahydrofuran or 2-methoxypropene.

Computed structures for protonated $[Fe^{II}–heme]$: The Car–Parrinello (CP) method, based on combining DFT with molecular dynamics (CPMD) provides a powerful approach in the study of biomolecular systems.[33] Besides the various heme models that have been successfully analyzed by CPMD,[11a,14b] the prototypical $[Fe^{II}–heme]$ complex has been examined by complete structural relaxation in three different spin states, with the triplet state found to have the lowest energy.[13] The comparison with the simplified FeP model has shown that the presence of vinyl, methyl, and propionate substituents on the porphyrin ring does not have any significant influence on the D_{4h} iron–porphyrin core of FeP, in terms of both structural and electronic features.[11a] In the lack of an X-ray structure of synthetic $[Fe^{II}–heme]$, its CPMD-optimized structure was used in the computational study of $[Fe^{II}–hemeH]^+$. Several isomers can be obtained in which a proton is formally placed on one of the distinct sites available. Figure 3 illustrates the numbering of carbon and oxygen atoms on the porphyrin ligand.

Henceforth, the convention is adopted that atom(no)H^+ will represent [Fe^{II}–heme] with an added H atom on

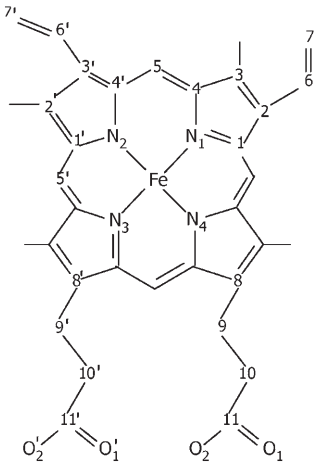

Figure 3. Atom-numbering convention used to define the position of the added hydrogen and the geometrical parameters of the computed [Fe^{II}–heme$H]^+$ isomers.

atom(no) and an overall positive charge. For example, O1H^+ stands for the species that is formally obtained by protonation of [Fe^{II}–heme] on the carbonyl oxygen that is labeled O1 in Figure 3. The relative energies of the various isomers depicted in Figure 4 are summarized in Table 3, while the list of structural parameters is provided in Table S1 of the Supporting Information.

The selected isomers do not include all possible species that can be obtained by protonating [Fe^{II}–heme] at the several nonequivalent protonation sites. The species listed in Table 3 and illustrated in Figure 4 are rather selected representatives of the structures that can be formed. For example C7H^+ has a counterpart in C7′H^+, both obtained by protonation at the β carbon atom of a vinyl group, O1H^+ is a close relative of O1′H^+, both being carbonyl-protonated species. The C7H^+ isomer, representative species formally derived from protonation at the β carbon atom of the vinyl group, is remarkably more stable than the one formed by protonation at the α carbon atom of the vinyl group, C6H^+. This finding is in agreement with the proton acceptor behavior of styrene, in which β protonation of the vinyl group yields a carbenium ion stabilized by electron release from the adjacent phenyl ring. The relative energy of C7H^+ yields a PA value of 1220 kJ mol^{-1} for neutral [Fe^{II}–heme]. The C2H^+ and C1H^+ isomers are formally obtained by protonation at the β and α carbon atoms of a pyrrole ring, respectively, and the former is significantly more stable. In free neutral pyrrole, the preferred protonation site is the α carbon atom, although favored by only a few kJ mol^{-1} with respect to the β carbon atom.[34] Obviously, the inclusion of the pyrrole unit in the anionic porphyrinato ligand causes profound changes in the electronic features and chemical properties of this moiety. The Fe-protonated species, FeH^+, is endowed with similar stability to C2H^+ and C5H^+, their

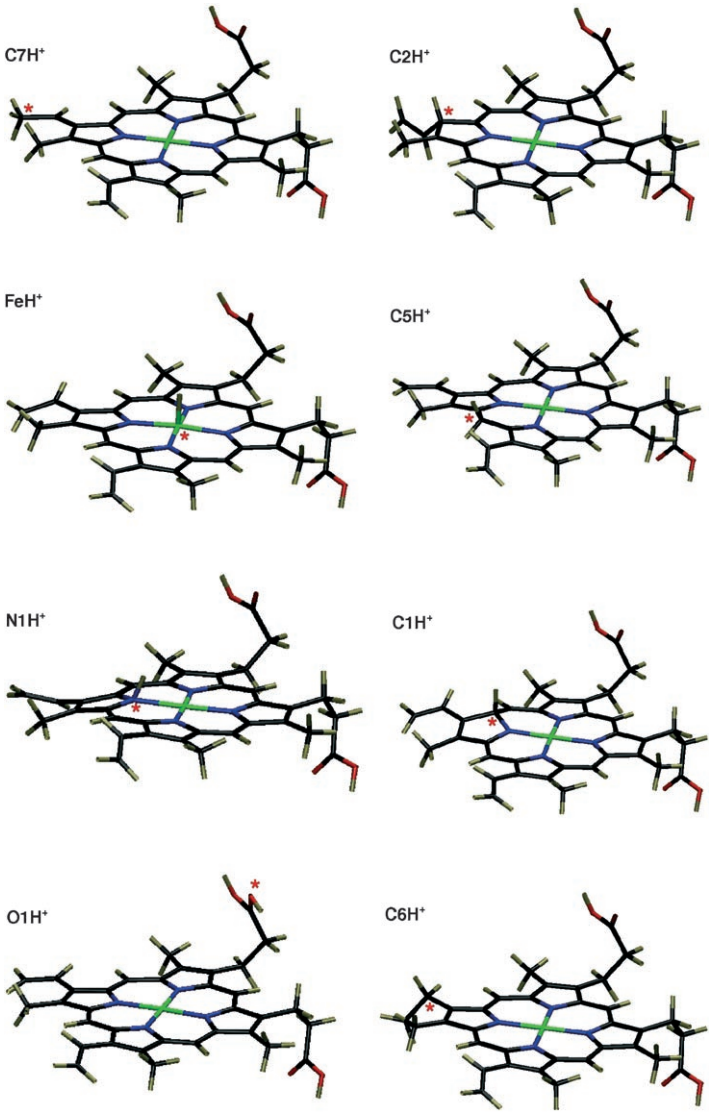

Figure 4. Optimized structures for [Fe^{II}–heme$H]^+$ ions. The asterisk marks the site of the additional proton.

Table 3. Relative energies of optimized structures of [Fe^{II}–heme$H]^+$ isomers.

Species	E_{rel}[a]	Species	E_{rel}[a]
C7H^+	0.0	N1H^+	86.9
C2H^+	57.7	C1H^+	103.7
FeH^+	61.9	O1H^+	142.1
C5H^+	63.5	C6H^+	160.1

[a] Relative energies (in kJ mol^{-1}) obtained by DFT calculations.

relative energies differing by less than 5 kJ mol^{-1}. It may be interesting to compare FeH^+ with protonated ferrocene, in which the comparable energy of the metal-protonated species and of an agostic structure with an additional interaction of the proton with one of the cyclopentadienyl rings is thought to account for the mobility of the proton.[35] However, in the present system, the iron site is quite remote from the C2 and C5 carbon atoms, which in turn are parted by

the α carbon atom of a pyrrole ring so that $[Fe^{II}$–hemeH$]^+$ should not be expected to undergo any rapid hydrogen migration or exhibit any fluxional behavior. The nitrogen-protonated species $N1H^+$ is markedly less stable than the thermodynamically favored isomer $C7H^+$, although its energy is comparable with that of the other next closely lying species, $C2H^+$, FeH^+, $C5H^+$, and $C1H^+$. Indeed, a nitrogen-protonated porphyrin intermediate has been suggested to play a role in cytochrome P450 chemistry by means of a hydrogen shuttle mechanism accounting for benzene hydroxylation.[9c] Finally, $O1H^+$ is the species formed if the proton is attached to the propionyl group. Protonation involves the carbonyl oxygen, known to be the favored protonation site in carboxylic acids.

The computational data can be further analyzed with respect to the spin-density distribution. Indeed, although spectroscopic methods for studies of paramagnetic molecules, such as electron spin resonance (ESR) and nuclear magnetic resonance (NMR) spectroscopy can provide information on the spin-density distributions for hemes, the most accurate means of gaining information about the spin delocalization appears to rely on quantum chemical calculations.[36] Figure 5 depicts the spin-density distribution in the most stable species, $C7H^+$, in few other low lying isomers, $C2H^+$, FeH^+, $C5H^+$, and in relatively higher energy species, $N1H^+$, $O1H^+$. Excess α spin density is represented in blue regions, whereas excess β spin is found in yellow areas.

As illustrated in Figure 5, the spin density distribution in $C7H^+$, the most stable isomer, shows an excess of α spin at the central iron atom. However, a peculiar feature in $C7H^+$ is the presence of a significant excess of β spin on the porphyrin frame. In particular, excess β spin is located on C6 so that the former vinyl group in protoporphyrin IX (P-IX) has acquired significant ethyl radical character. The situation can be described as arising from the transfer of an electron from Fe^{II} to the protonated porphyrin system as depicted in the inset of Figure 5. Integration of the spin density on the porphyrin gives a total of 0.55 electrons for the net-charge transfer from the iron to the porphyrin, which corresponds to an intermediate situation between $[Fe^{II}$–$HemeH^+]$ and $[Fe^{III}$–$hemeH^{\bullet}]^+$. Therefore, a comprehensive view of $C7H^+$, representing the most stable isomer of protonated heme, should include a contribution with iron(III) character at the metal center and radical character in proximity of the added hydrogen.

A certain contribution of an electronic structure corresponding to $[Fe^{III}$–$hemeH^{\bullet}]^+$ is clearly manifest also in the other isomers examined (as shown by the spin-density distributions depicted in Figure 5). A noticeable exception, namely a species lacking any significant porphyrin-based radical character, is presented by the Fe-protonated, N-protonated, and O-protonated isomers, FeH^+, $N1H^+$, and $O1H^+$, respectively. In the first two cases (FeH^+ and $N1H^+$), there are two unpaired electrons mainly localized on the iron atom, as in neutral $[Fe^{II}$–heme]. In the last case ($O1H^+$), there is partial electron transfer from the iron to the protonated carboxyl moiety.

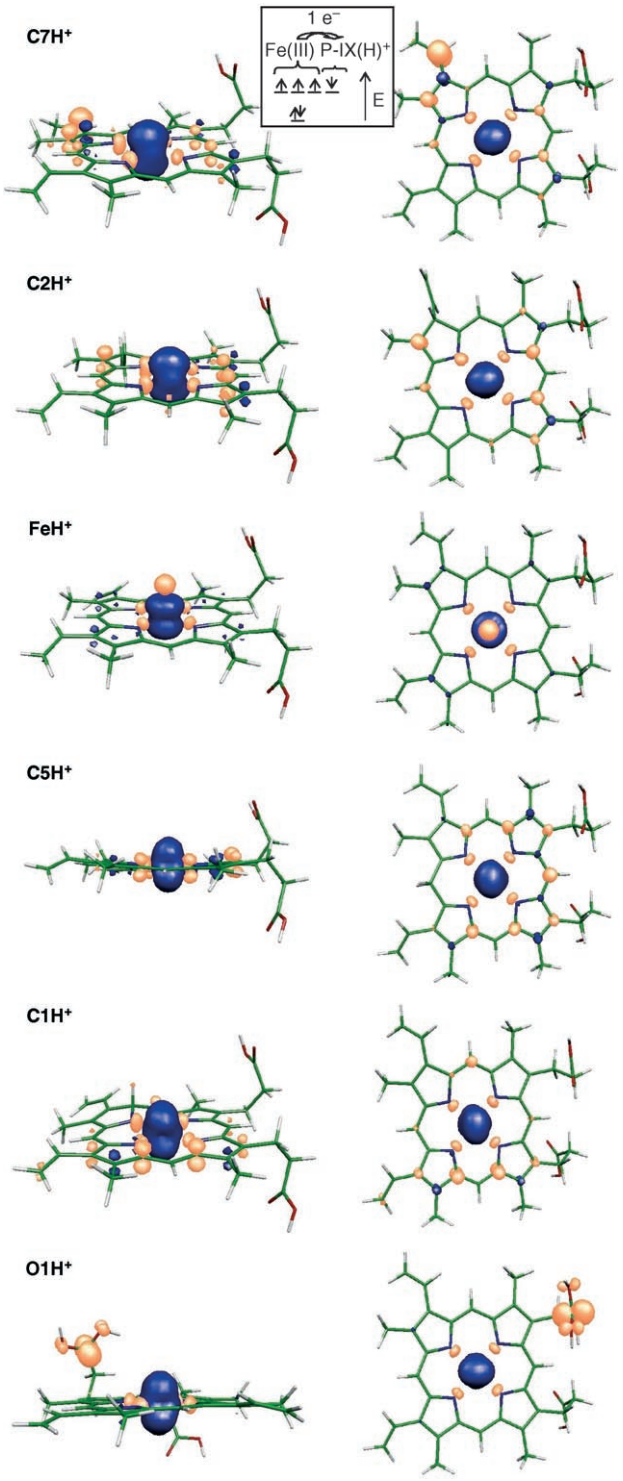

Figure 5. Side and top view of the spin distribution in exemplary isomers of $[Fe^{II}$–hemeH$]^+$ ions. Blue regions denote excess α and yellow areas excess β density.

Discussion

The $[Fe^{II}$–hemeH$]^+$ species, hitherto named protonated heme, poses several interesting questions in spite of its ap-

parent simplicity. The first question regards the site of proton attachment. In the present case, the ions centered at *m*/*z*: 617, formally corresponding to $[Fe^{II}–hemeH]^+$, are not the product of a simple proton-transfer reaction to free heme, rather being formed by a dissociation process from a precursor owning a covalently bound heme group. A useful tool to obtain an insight into the site of protonation, the number of labile hydrogens, and the possible mobility of hydrogen over multiple sites is based on H/D-exchange reactions. When $[Fe^{II}–hemeH]^+$ ions are exposed to a gaseous exchange reagent, such as CD_3CO_2D, one observes incorporation of D atoms, their number never exceeding two. The incorporation of these two D atoms reaches an equilibrium in which the isotopic ion abundances reflect the effective D content of the exchange reagent in the reaction cell. The same extent of D incorporation is observed when ND_3 is used, namely in the presence of a reagent of higher basicity and higher number of exchangeable D atoms, besides higher D isotope content in the conditions of the experiments. This constant number of two H/D exchanges is also verified for $[Fe^{III}–heme]^+$ ions. Moreover, when both $[Fe^{II}–hemeH]^+$ and $[Fe^{III}–heme]^+$ ions are obtained from a CH_3OD solution of their neutral precursors, hemin chloride and microperoxidase, respectively, their mass analysis reveals once again that only two D atoms are incorporated from the solvent and the so-obtained deuterated species are further unreactive with ND_3 in the FTICR cell. The combined evidence speaks in favor of an exchange process involving the hydroxyl groups of the propionyl substituents, known to be exchangeable sites in solution. At the same time, the possibility may be discarded that the carboxyl groups are the stable protonation sites. In this case, the hydrogen atoms expected to undergo exchange should include the former two hydroxyl hydrogens of neutral heme and the added proton, making a total of three. Thus, it is inferred that the H/D-exchange process involves the neutral propionyl groups at the periphery of the positively charged heme-type ions. This conclusion is confirmed by the single D-atom incorporation when one of the propionyl groups is turned into a methyl ester. The two likely mechanisms by which the H/D-exchange process may occur in the present system are described in the landmark paper by Campbell et al.,[29a] with betaine ($(HO)CO–CH_2–N(CH_3)_3^+$) as the model system. In the first mechanism, an intermediate zwitterion is formed (as in the so-called salt bridge mechanism), as depicted in Equation (4) in which the carboxyl group undergoing H/D exchange is shown. The CO_2H group is bound to the remaining portion (R^+) of $[Fe^{II}–hemeH]^+$ or $[Fe^{III}–heme]^+$.

$$R^+CO_2H + ND_3 \rightarrow [R^+CO_2H\ ND_3] \rightarrow [R^+CO_2^-ND_3H^+] \rightarrow [R^+CO_2D\ ND_2H] \rightarrow R^+CO_2D + ND_2H \quad (4)$$

In the second mechanism a "flip-flop" exchange is operating; this is depicted in Equation 5, which shows CD_3CO_2D as the exchange reagent. Acetic acid is in fact known to be prone to undergoing a multicenter exchange in the hydrogen bonded dimer.[29a]

$$R^+\text{-}CO_2H + CD_3CO_2D \rightarrow \left(R^+\text{-}C(=O\cdots D\text{-}O)(O\text{-}H\cdots O=)C\text{-}CD_3 \right) \rightarrow R^+\text{-}CO_2D + CD_3CO_2H \quad (5)$$

The experimental data available do not enable us to discriminate between these two pathways, which is beyond the scope of the present study. However, the distinctly higher reactivity of the stronger base ND_3 suggests a mechanism for this molecule involving a net proton transfer event within the collision complex [Eq. (4)]. In either mechanism the H/D exchange is activated by the energy released in the ion neutral complex by electrostatic and hydrogen-bond interactions. The conclusion common to both $[Fe^{II}–hemeH]^+$ and $[Fe^{III}–heme]^+$ ions is then that the H atoms undergoing exchange belong to the propionyl functionalities and are therefore relatively far apart in the molecular frame. A question may rise as to whether the exchange reagent may sample both sites within the same ion neutral complex. Assuming that this condition holds, the rate constants for the stepwise exchanges that were obtained by a kinetic fitting program have been statistically corrected yielding the values reported in italics in Table 1. The corrected k_1 and k_2 values turn out to be very close, as expected for the reaction of two equivalent sites undergoing H/D equilibration with the exchange reagent in a relatively long-lived complex. It is interesting to note that the remaining portion (R^+) of $[Fe^{II}–hemeH]^+$ or $[Fe^{III}–heme]^+$, differing for the formal oxidation state of iron and for the presence of an additional H atom, does affect to some extent the kinetics of H/D exchange. Their rates are consistently faster for $[Fe^{III}–heme]^+$ by a factor of approximately two.

The site of H attachment in $[Fe^{II}–hemeH]^+$: Given the scant information provided by H/D-exchange reactions on the site of H attachment in $[Fe^{II}–hemeH]^+$, which are found to occur on the neutral carboxylic groups, one may resort to the results of DFT calculations performed on a number of isomers exemplifying various species that may be obtained by protonation of neutral heme. The thermodynamically favored isomer among the investigated structures is the one formally obtained by protonation at the β carbon atom of a vinyl group (C7H$^+$ in Figure 4). In the resulting species, the π-electron framework of the porphyrin ligand is relatively unperturbed and in a suitable geometrical arrangement for orbital interaction with the formally vacant p orbital developing on C6. As already noted, this isomer is characterized by a peculiar spin-density distribution (Figure 5, top). In fact, this most stable isomer of $[Fe^{II}–hemeH]^+$ displays electronic features that may be ascribed in part to $[Fe^{III}–hemeH^{\bullet}]^+$, showing that protonation of the porphyrinato ligand at C7 is accompanied by substantial electronic reorganization, producing an iron atom with partial character of iron(III) and partial radical character at the former vinyl

substituent. The electron affinity of the porphyrin π system and the relative stability of iron(III) may account for these features. In such a case, the ligand behaves as noninnocent, lacking a definite closed-shell configuration.[37] It can be argued that given the origin of these ions, produced by collision-induced dissociation accompanying ESI of microperoxidase, it is conceivable to obtain heme-type ions with iron(III), namely iron in the same oxidation state as in the microperoxidase precursor. It is obvious, however, that the electronic properties of the optimized structure obtained from the calculation do not depend on the specific formation pathway of protonated heme.

Regarding the gas-phase ion chemistry of $[Fe^{II}–hemeH]^+$, in reactions other than H/D exchange, the porphyrinato ligand is apparently not directly involved. As expected considering the high PA of $[Fe^{II}–heme]$, none of the bases investigated were found to be able to abstract a proton. Indeed, if the neutral carboxyl substituents partake in H/D exchange with ammonia by a reversible H^+/D^+ transfer mechanism within the collision complex, it is reasonable to envisage these groups as the most acidic sites. In ligand addition reactions involving the metal center, $[Fe^{II}–hemeH]^+$ shows a reactivity different to some extent from that of $[Fe^{III}–heme]^+$. Lewis bases, such as CD_3CO_2D, ND_3 and $(C_2H_5O)_3P$ show less, if any, reactivity with $[Fe^{II}–hemeH]^+$. $(C_2H_5O)_3P$ is the least disfavored ligand in the comparative assay, in agreement with its soft character which provides enhanced affinity for iron(II) with respect to iron(III). However, it is only with NO that the relative reactivity order shows an inversion in favor of $[Fe^{II}–hemeH]^+$. This finding provides circumstantial evidence for an iron with iron(II) character. The reactivity of NO for iron(III) is in fact generally found to be lower than that for iron(II). For example, in water solution the ferrous complex $[Fe^{II}–TPPS]$ (TPPS = tetra(4-sulfonato-phenyl)porphinato) reacts with NO about 10^3 times faster than does the ferric analogue.[38] Interestingly, however, the reactivity of the ferric complex, which is present in the form $[Fe^{III}–TPPS(H_2O)_2]$, conforms to a substitution mechanism dominated by the dissociation of an axial water ligand, so that metal–NO bond formation requires prior ligand displacement. High spin ferroheme protein complexes are often five coordinated and their typically higher reactivity than the ferriheme analogues towards ligand association has been suggested to derive from the free coordination site. In this respect, the present gas-phase reactivity data provide a measure of the intrinsic reactivity towards NO association. Both $[Fe^{III}–heme]^+$ and $[Fe^{II}–hemeH]^+$ ions are four-coordinate and their kinetics of ligand association are obviously unaffected by any axial ligand.

Conclusion

Establishing the features of naked protonated heme was the primary goal of the present work combining both an experimental study and theoretical calculations. Though seemingly straightforward, the survey of protonated heme presents unexpected facets. The calculated most stable species corresponding to $[Fe^{II}–hemeH]^+$ is found to hold the additional H atom on the β carbon atom of a vinyl group. The relative stability of this species accounts for a PA value of 1220 kJ mol^{-1} for $[Fe^{II}–heme]$. In agreement with this high PA, the three β hydrogens of the protonated vinyl group do not partake in H/D-exchange processes, a reaction that occurs rather on the neutral carboxylic groups, displaying reactivity features resembling those exhibited by $[Fe^{III}–heme]^+$. Indeed, in both ions the exchange reaction affects the same uncharged groups at the periphery of the porphyrin ring. Representative isomers formally corresponding to protonated heme, $[Fe^{II}–hemeH]^+$, have been investigated by DFT computations and the analysis of the spin-density distribution in the most stable $C7H^+$ isomer of $[Fe^{II}–hemeH]^+$ shows substantial radical character on the α carbon atom of the former vinyl group. This finding implies that a complete description of protonated heme should include a contribution of $[Fe^{III}–hemeH^{\bullet}]^+$. The reactivity of $[Fe^{II}–hemeH]^+$ and $[Fe^{III}–heme]^+$ ions towards ligand association, however, is quite distinct, as expected for a metal-directed reaction. The addition reaction with NO deserves special mention. $[Fe^{II}–hemeH]^+$ and $[Fe^{III}–heme]^+$ ions show a comparable efficiency reacting as naked ions in the gas phase, in contrast with the enhanced reactivity of iron(II) complexes in solution when compared with iron(III) counterparts. This result may be ascribed to the $[Fe^{III}–hemeH^{\bullet}]^+$ character of protonated heme but may also be a consequence of the free axial sites available in both complexes in the gas phase.

Interestingly, the metal-ion oxidation state in the multicharged ions of heme proteins has been related to its H-atom content, implying that each additional hydrogen, added as a proton, will contribute to the overall charge, adding up to the positive charge of +2/+3 associated with iron(II/III).[39] The present study of the simple species formally corresponding to protonated $[Fe^{II}–heme]$ spells a word of caution on this generalization.

Experimental Section

FTICR mass spectrometry: Experiments were performed with a FTICR Bruker Spectrospin 47e mass spectrometer upgraded to BioApex with an Analytica of Branford Electrospray Ionization (ESI) source. Ions formed in the ESI source are transferred by an ion guide into a cylindrical "infinity" cell placed in the high-field region of a 4.7 T superconducting magnet. Needle valves enable neutral compounds to be admitted into the cell at a constant pressure in the range of $0.5–12\times10^{-8}$ mbar. The pressure readings, obtained from a cold cathode sensor (IKR Pfeiffer Balzers S.p.A., Milan, Italy), were calibrated by using the rate constant $k = 1.1\times10^{-9}$ cm^3 s^{-1} for the reference reaction $CH_4^{+\bullet} + CH_4 \rightarrow CH_5^+ + CH_3^{\bullet}$ and corrected by utilizing individual response factors.[40] Uncertainties in pressure measurements, estimated to be ±30%, are the major source of error in the reported rate constants. Because the inlets and the cell of the spectrometer are typically contaminated by traces of water, care was taken to avoid depletion of the deuterium content of the deuterated reagents used. Prior to using them, the inlet system and the cell are primed overnight with D_2O (approximately 10^{-6} mbar) to allow for the complete exchange of all surfaces. D_2O is then thoroughly pumped away. The iso-

topic content of the deuterating agents admitted at constant pressure in the FTICR cell is checked from their mass spectrum obtained by electron ionization using the internal filament. Although the reagent compounds have a stated high isotopic purity (=99 atom%) the percent deuterium in the cell is not as high.

Sample 10 μM solutions are prepared containing either hemin chloride in methanol or microperoxidase (MP11) in 1:1 aqueous methanol with 2% acetic acid. The solutions are continuously sprayed at a 2 $\mu l\,min^{-1}$ flow rate by a syringe pump. A countercurrent flow of heated dry gas (nitrogen at 130°C) is used to desolvate the ions. After an accumulation interval of 0.5 s in a rf-only hexapole, the ion population is pulsed into the ICR cell at room temperature (300 K). ESI of hemin chloride yields gaseous $[Fe^{III}$–heme$]^+$ ions at nominal m/z: 616, whereas $[Fe^{II}$–hemeH$]^+$ ions (m/z: 617) are obtained by collision-induced dissociation of MP11 ions applying a high capillary to skimmer potential difference.

Ion ejection procedures are routinely adopted in FTICR mass spectrometry to select ions at a single m/z ratio and observe their ion chemistry with the neutral admitted into the cell. However, to avoid unintended off-resonance excitation[41] of the reactant ion, it was decided to restrict the use of radio frequency ejection techniques, selecting the whole isotopic cluster corresponding to the heme-type ion and allowing it to undergo reaction. In the study of H/D-exchange reactions, data analysis faces the problem of deconvoluting the isotopic natural abundance distribution in the mass spectra of variously deuterated species.[26] In the H/D-exchange experiments, the relative amounts of ions with varying D content were calculated in each mass spectrum by subtracting all isotopic contributions from the raw data according to their natural abundances. The so-obtained relative abundances were analyzed as a function of reaction time to extract kinetic information. Similarly, ligand addition reactions were studied by recording the time dependence of the relative ion abundances for both the reagent ion and the association product. In the case of both H/D exchange and ligand addition reactions, the slope of the semilogarithmic plot of the reagent ion abundance versus reaction time yields a pseudo-first-order rate constant (k_{obs}), which is divided by the concentration of the neutral reagent to afford the second-order rate constant (k_{exp}) for the bimolecular exchange reaction. Alternatively, rate constants were obtained by fitting the time dependence of the reagent and product ion abundances using the program KinFit.[31]

The products D_2O (99.9 atom% deuterium), CD_3CO_2D (99.5 atom% deuterium), ND_3 (99.0 atom% deuterium), CH_3OD (99.5 atom% deuterium), methanol, NO, $(C_2H_5O)_3P$, hemin chloride, and microperoxidase (MP11) are from commercial sources (Sigma Aldrich, Italy; Matheson Gas) and were used as received.

Computational details: The initial structures for the calculation of $[Fe^{III}$–hemeH$]^+$ were taken from the optimized structure of $[Fe^{III}$–heme], obtained in our previous work.[13] Extra hydrogen atoms were attached to several putative heme protonation sites corresponding to different types of carbon atoms: alpha pyrrole (C1), beta pyrrole (C2), alpha vinyl (C6), beta vinyl (C7), and meso carbon atom (C5) (Figure 3). Protonation at one pyrrole nitrogen (N1), at one carboxyl oxygen (O1), and at the iron was also considered.

The calculations were carried out by using the Car–Parrinello molecular dynamics method,[33a] as implemented in the CPMD code.[33b–d] The Kohn–Sham orbitals are expanded in a plane wave (PW) basis set with the kinetic energy cutoff of 70Ry. Earlier calculations on iron–porphyrin models[11a,12a–b] showed that this cutoff is sufficient for achieving a good convergence of energies and structural properties. The systems were enclosed in an orthorombic supercell of size $18\times18\times13$ $Å^3$ periodically repeated in space. Ab initio pseudopotentials, generated within the Troullier–Martins scheme,[42] including the nonlinear core correction[43] for the iron atom were employed. Calculations were made by using the generalized gradient-corrected approximation of the spin-dependent density functional theory (DFT-LSD), following the method of Becke and Perdew.[44] Structure optimizations on the triplet ground state were performed by means of molecular dynamics with annealing of the atomic velocities, by using a time step of 0.072 fs and a value of 700 a.u. for the fictitious electronic mass of the Car–Parrinello Lagrangian. The proton affinitiy of the heme group was computed from the differential energy between the protonated and unprotonated form, each one in its own minimum energy structure. Previous work has demonstrated the reliability of this computational setup in the description of structural, energetic, and dynamical properties of heme-based systems.[11a,12a–b] In particular, the structure and spin states of an iron–porphyrin were found to be in agreement with previous all-electron calculations[45] as well as with more recent studies.[46] The performance of different exchange and correlation functionals in the modeling of heme systems was analyzed by Scherlis et al.[47] Structure analysis was performed with the variational density matrix method (VMD).[48]

Acknowledgements

This project was supported by the Italian Ministero dell′ Istruzione, dell′ Università e della Ricerca, and by the Generalitat de Catalunya (2005SGR-00036) and the Ministerio de Educación y Ciencia (MEC) (FIS2005–00655). Computer resources were provided by the Barcelona Supercomputing Center (BSC). C.R. acknowledges a Ramón y Cajal contract from the MEC.

[1] W. Kaim, B. Schwederski, *Bioinorganic Chemistry: Inorganic Elements in the Chemistry of Life*, Wiley, Chichester, **1994**.
[2] S. J. Lippard, J. M. Berg, *Principles of Bioinorganic Chemistry*, University Science Books, Mill Valley, CA, **1994**.
[3] a) G. Ashkenasy, D. Cahen, R. Cohen, A. Shanzer, A. Vilan, *Acc. Chem. Res.* **2002**, *35*, 121–128; b) D. G. Wu, D. Cahen, P. Graf, R. Naaman, A. Nizan, D. Shvarts, *Chem. Eur. J.* **2001**, *7*, 1743–1749; c) G. Ashkenasy, A. Ivanisevic, R. Cohen, C. E. Felder, D. Cahen, A. B. Ellis, A. Shanzer, *J. Am. Chem. Soc.* **2000**, *122*, 1116–1122; d) E. Katz, V. Heleg-Shabtai, I. Willner, H. Rau, W. Haehnel, *Angew. Chem.* **1998**, *110*, 3443–3447; *Angew. Chem. Int. Ed.* **1998**, *37*, 3253–3256; e) K. S. Suslick, P. Bhyrappa, J.-H. Chou, M. E. Kosal, S. Nakagaki, D. W. Smithenry, S. R. Wilson, *Acc. Chem. Res.* **2005**, *38*, 283–291.
[4] G. H. Loew, D. L. Harris, *Chem. Rev.* **2000**, *100*, 407–419.
[5] B. Meunier, A. Robert, G. Pratviel, J. Bernardou in *Porphyrin Handbook, Vol. 4*, (Eds.: K. M. Kadish, K. M. Smith, R. Guilard), Academic Press, San Diego, **2000**, pp. 119–187.
[6] A. Lombardi, F. Nastri, V. Pavone, *Chem. Rev.* **2001**, *101*, 3165–3189.
[7] B. Meunier, S. P. de Visser, S. Shaik, *Chem. Rev.* **2004**, *104*, 3947–3980.
[8] W.-D. Woggon, *Acc. Chem. Res.* **2005**, *38*, 127–136.
[9] a) C. Li, W. Wu, D. Kumar, S. Shaik, *J. Am. Chem. Soc.* **2006**, *128*, 394–395; b) S. P. de Visser, D. Kumar, S. Cohen, R. Shacham, S. Shaik, *J. Am. Chem. Soc.* **2004**, *126*, 8362–8363; c) S. P. de Visser, S. Shaik, *J. Am. Chem. Soc.* **2003**, *125*, 7413–7424; d) C. M. Bathelt, L. Ridder, A. J. Mulholland, J. N. Harvey, *J. Am. Chem. Soc.* **2003**, *125*, 15004–15005; e) S. Shaik, D. Kumar, S. P. de Visser, A. Altun, W. Thiel, *Chem. Rev.* **2005**, *105*, 2279–2328.
[10] H. Lin, J. C. Schoeneboom, S. Cohen, S. Shaik, W. Thiel, *J. Phys. Chem. B* **2004**, *108*, 10083–10088.
[11] a) C. Rovira, K. Kunc, J. Hutter, P. Ballone, M. Parrinello, *J. Phys. Chem. A* **1997**, *101*, 8914–8925; b) N. Matsuzawa, M. Ata, D. A. Dixon, *J. Phys. Chem.* **1995**, *99*, 7698–7706; c) S. Obara, H. Kashiwagi, *J. Chem. Phys.* **1982**, *77*, 3155; d) M.-S. Liao, S. Scheiner, *J. Comput. Chem.* **2002**, *23*, 1391–1403; e) J.-D. Marechal, G. Barea, F. Maseras, A. Lledos, L. Mouawad, D. Perahia, *J. Comput. Chem.* **2000**, *21*, 282–294; f) Y. Zhang, J. Mao, N. Godbout, E. Oldfield, *J. Am. Chem. Soc.* **2002**, *124*, 13921–13930; g) M. P. Johansson, D. Sundholm, G. Gerfen, M. Wikstroem, *J. Am. Chem. Soc.* **2002**, *124*, 11771–11780; h) H. Hirao, S. Shaik, P. M. Kozlowski, *J. Phys. Chem. A* **2006**, *110*, 6091–6099.
[12] a) C. Rovira, P. Ballone, M. Parrinello, *Chem. Phys. Lett.* **1997**, *271*, 247–250; b) C. Rovira, M. Parrinello, *Biophys. J.* **2000**, *78*, 93–100;

c) T. Wondimagegn, A. Ghosh, *J. Am. Chem. Soc.* **2001**, *123*, 5680–5683; d) A. Ghosh, D. F. Bocian, *J. Phys. Chem.* **1996**, *100*, 6363–6367; e) G. B. Richter-Addo, R. A. Wheeler, C. A. Hixson, L. Chen, M. A. Khan, M. K. Ellison, C. E. Schulz, W. R. Scheidt, *J. Am. Chem. Soc.* **2001**, *123*, 6314–6326.
[13] C. Rovira, M. Parrinello, *Chem. Eur. J.* **1999**, *5*, 250–262.
[14] a) D. M. A. Smith, M. Dupuis, E. R. Vorpagel, T. P. Straatsma, *J. Am. Chem. Soc.* **2003**, *125*, 2711–2717; b) C. Rovira, P. Carloni, M. Parrinello, *J. Phys. Chem. B* **1999**, *103*, 7031–7035; c) A. R. Groenhof, M. Swart, A. W. Ehlers, K. Lammertsma, *J. Phys. Chem. A* **2005**, *109*, 3411–3417; d) A. S. Galstyan, S. D. Zariæ, E.-W. Knapp, *J. Biol. Inorg. Chem.* 2005, 10, 343–354; e) K. P. Jensen, U. Ryde, *ChemBioChem* **2003**, *4*, 413–424; f) J. M. Ugalde, B. Dunietz, A. Dreuw, M. Head-Gordon, R. J. Boyd, *J. Phys. Chem. A* **2004**, *108*, 4653–4657.
[15] a) S. Franzen, *Proc. Natl. Acad. Sci. USA* **2002**, *99*, 16754–16759; b) D. P. Linder, K. R. Rodgers, J. Banister, G. R. A. Wyllie, M. K. Ellison, W. R. Scheidt, *J. Am. Chem. Soc.* **2004**, *126*, 14136–14148; c) D. P. Linder, K. R. Rodgers, *Inorg. Chem.* **2005**, *44*, 1367–1380; d) N. J. Silvernail, A. Roth, C. E. Shulz, B. C. Noll, W. R. Scheidt, *J. Am. Chem. Soc.* **2005**, *127*, 14422–14433; e) K. P. Jensen, U. Ryde, *J. Biol. Chem.* **2004**, *279*, 14561–14569; f) D. D. Klug, M. Z. Zgierski, J. S. Tse, Z. Liu, J. R. Kincaid, K. Czarnecki, R. J. Hemley, *Proc. Natl. Acad. Sci. USA* **2002**, *99*, 12526–12530; g) I. V. Novozhilova, P. Coppens, J. Lee, G. B. Richter-Addo, K. A. Bagley, *J. Am. Chem. Soc.* **2006**, *128*, 2093–2104.
[16] a) D. P. Ridge in *Unimolecular and Bimolecular Reaction Dynamics* (Eds.: C. Y. Ng, T. Baer, I. Powis), Wiley, Chichester, **1994**, Chapter 7, pp. 337–370; b) D. P. Ridge in *Fundamentals and Applications of Gas Phase ion Chemistry* (Ed.: K. R. Jennings), Kluwer, Dordrecht, **1999**, pp. 475–476.
[17] a) K. K. Irikura, J. L. Beauchamp, *J. Am. Chem. Soc.* **1991**, *113*, 2767–2768; b) S. Kazazic, L. Klasinc, S. P. McGlynn, D. Srzic, M. G. H. Vicente, *J. Phys. Chem. A* **2004**, *108*, 10997–11000.
[18] Y. Shen, U. Ryde, *Chem. Eur. J.* **2005**, *11*, 1549–1564.
[19] a) O. Chen, S. Groh, A. Liechty, D. P. Ridge, *J. Am. Chem. Soc.* **1999**, *121*, 11910–11911; b) L. A. Hayes, A. M. Chappell, E. E. Jellen, V. Ryzhov, *Int. J. Mass Spectrom.* **2003**, *227*, 111–120; c) F. Angelelli, B. Chiavarino, M. E. Crestoni, S. Fornarini, *J. Am. Soc. Mass Spectrom.* **2005**, *16*, 589–598.
[20] V. A. Pashynska, H. Van den Heuvel, M. Claeys, M. V. Kosevich, *J. Am. Soc. Mass Spectrom.* **2004**, *15*, 1181–1190.
[21] Y. T. Li, Y. L. Hsieh, J. D. Henion, B. Ganem, *J. Am. Soc. Mass Spectrom.* **1993**, *4*, 631–637.
[22] J. M. Wells, G. E. Reid, B. J. Engel, P. Pan, S. A. McLuckey, *J. Am. Soc. Mass Spectrom.* **2001**, *12*, 873–876.
[23] F. He, C. L. Hendrickson, A. G. Marshall, *J. Am. Soc. Mass Spectrom.* **2000**, *11*, 120–126.
[24] a) P. Ausloos, S. G. Lias, *J. Am. Chem. Soc.* **1981**, *103*, 3641–3647; b) C. H. DePuy, V. M. Bierbaum, *Acc. Chem. Res.* **1981**, *14*, 146–153.
[25] S. G. Lias, *J. Phys. Chem.* **1984**, *88*, 4401–4407.
[26] a) C. Lifshitz, *Int. J. Mass Spectrom.* **2004**, *234*, 63–70; b) Z. Zhang, S. Guan, A. G. Marshall, *J. Am. Soc. Mass Spectrom.* **1997**, *8*, 659–670.
[27] a) M. K. Green, C. B. Lebrilla, *Mass Spectrom. Rev.* **1997**, *16*, 53–71; b) J. C. Jurchen, R. E. Cooper, E. R. Williams, *J. Am. Soc. Mass Spectrom.* **2003**, *14*, 1477–1487; c) E. H. Gur, L. J. de Koning, N. M. M. Nibbering, *J. Am. Soc. Mass Spectrom.* **1995**, *6*, 466–477.
[28] E. P. Hunter, S. G. Lias in *NIST Chemistry Webbook*, *NIST Standard Reference Database Number 69* (Eds.: P. J. Linstrom, W. G. Mallard), National Institute of Standards and Technology, Gaithersburg, MD, **2003**, http://webbook.nist.gov.
[29] a) S. Campbell, M. T. Rodgers, E. M. Marzluff, J. L. Beauchamp, *J. Am. Chem. Soc.* **1995**, *117*, 12840–12854; b) X. Cheng, C. Fenselau, *Int. J. Mass Spectrom. Ion Processes* **1992**, *122*, 109–119.
[30] T. Su, W. J. Chesnavich, *J. Chem. Phys.* **1982**, *76*, 5183–5185.
[31] N. Z. Shen, R. M. Pope, D. V. Dearden, *Int. J. Mass Spectrom.* **2000**, *196*, 639–652.
[32] E. D. Nelson, R. Li, H. I. Kenttämaa, *Int. J. Mass Spectrom.* **1999**, *185/186/187*, 91–96.
[33] a) R. Car, M. Parrinello, *Phys. Rev. Lett.* **1985**, *55*, 2471–2474; b) CPMD program, Copyright IBM, **1990–2003**, Copyright MPI für Festkörperforschung, Stuttgart, **1997–2001**, http://www.cpmd.org; c) D. Marx, J. Hutter, *Ab Initio Molecular Dynamics: Theory and Implementation in Modern Methods and Algorithms of Quantum Chemistry* (Ed.: J. Grotendorst), John von Neumann Institute for Computing, Julich, Germany, **2000**, 301–409; d) P. Carloni, U. Rothlisberger, M. Parrinello, *Acc. Chem. Res.* **2002**, *35*, 455–464.
[34] V. Q. Nguyen, F. Tureèek, *J. Mass Spectrom.* **1996**, *31*, 1173–1184.
[35] a) M. Bühl, S. Grigoleit, *Organometallics* **2005**, *24*, 1516–1527; b) M. J. Mayor-Lopez, H. P. Lüthi, H. Koch, P. Y. Morgantini, J. Weber, *J. Chem. Phys.* **2000**, *113*, 8009–8014; c) A. Irigoras, J. M. Mercero, I. Silanes, J. M. Ugalde, *J. Am. Chem. Soc.* **2001**, *123*, 5040–5043.
[36] a) M. P. Johansson, D. Sundholm, G. Gerfen, M. Wikström, *J. Am. Chem. Soc.* **2002**, *124*, 11771–11780; b) F. A. Walker, *Coord. Chem. Rev.* **1999**, *185–186*, 471–534.
[37] P. Chaudhuri, C. N. Verani, E. Bill, E. Bothe, T. Weyhermüller, K. Wieghardt, *J. Am. Chem. Soc.* **2001**, *123*, 2213–2223.
[38] a) P. C. Ford, L. E. Laverman, *Coord. Chem. Rev.* **2005**, *249*, 391–403; b) M. Hoshino, L. E. Laverman, P. C. Ford, *Coord. Chem. Rev.* **1999**, *187*, 75–102.
[39] F. He, C. L. Hendrickson, A. G. Marshall, *J. Am. Soc. Mass Spectrom.* **2000**, *11*, 120–126.
[40] a) V. A. Anicich, *J. Phys. Chem. Ref. Data* **1993**, *22*, 1469–1569; b) J. E. Bartmess, R. M. Georgiadis, *Vacuum* **1983**, *33*, 149–153.
[41] J. W. Gauthier, T. R. Trautman, D. B. Jacobson, *Anal. Chim. Acta* **1991**, *246*, 211–225.
[42] M. Troullier, J. L. Martins, *Phys. Rev. B* **1991**, *43*, 1993–2006.
[43] S. G. Louie, S. Froyen, M. L. Cohen, *Phys. Rev. B* **1982**, *26*, 1738–1742.
[44] a) A. D. Becke, *J. Chem. Phys.* **1986**, *84*, 4524–4529; b) J. P. Perdew, *Phys. Rev. B* **1986**, *33*, 8822–8824.
[45] a) B. Delley, *Physica B* **1991**, *172*, 185–193; b) N. Matsuzawa, M. Ata, D. A. Dixon, *J. Phys. Chem.* **1995**, *99*, 7698–7706.
[46] M.-S. Liao, S. Scheiner, *J. Chem. Phys.* **2002**, *116*, 3635–3645.
[47] D. A. Scherlis, D. A. Estrin, *Int. J. Quantum Chem.* **2001**, *87*, 158–166.
[48] W. Humphrey, A. Dalke, K. Schulten, *J. Mol. Graphics* **1996**, *14*, 33–38.

Received: May 29, 2006
Published online: October 16, 2006

